Propelling and spinning of microsheets in nematic liquid crystals driven by ac electric field

M. V. Rasna,[1] U. V. Ramudu,[2] R. Chandrasekar,[2] and Surajit Dhara[1,*]
[1]*School of Physics, University of Hyderabad, Hyderabad-500046, India*
[2]*School of Chemistry, University of Hyderabad, Hyderabad-500046, India*
(Received 23 November 2016; published 30 January 2017)

Dynamics of microparticles in isotropic liquids by transducing the energy of an applied electric field have been studied for decades. Recently, such studies in anisotropic media like liquid crystals have opened up new perspectives in colloid science. Here, we report studies on ac-electric-field-driven dynamics of microsheets in nematic liquid crystals. In planar aligned liquid crystals, with negative dielectric anisotropy, the microsheets are propelled parallel to the director. A steady spinning of the microsheets is observed in homeotropic cells with positive dielectric anisotropy liquid crystals. The velocity of propelling and the angular frequency of spinning depends on the amplitude and the frequency of the applied electric field. The electrokinetic studies of anisotropic microparticles are important as they are potential for applications in microfluidics and in areas where the controlled transport or rotation is required.

DOI: 10.1103/PhysRevE.95.012710

I. INTRODUCTION

Study on the externally driven dynamics of colloidal particles is an active research field in soft matter science. Most commonly used media for dispersing colloidal particles are the isotropic liquids, like water, and the common driving force for particle dynamics is the electric field. The electrokinetic phenomena are exploited in microfluidic devices and electrophoretic displays [1–3]. They are mostly described by induced charge electrophoresis (ICEP) and induced charge electroosmosis (ICEO). The ICEP is assigned to the particle motion driven by the ICEO flow around the particle. The ICEP leads to the transport and rotation of freely suspended colloidal particles [4–11]. In the isotropic medium, for the particle to be electrokinetically active, it must be charged or asymmetric [6,7]. However, in anisotropic medium like liquid crystals some interesting phenomena with spherically symmetric and neutral microparticles are reported. This includes nonlinear electrophoresis of dielectric and metal microspheres, backflow-induced transport of particles associated with the director realignment, linear and nonlinear electrophoresis, Quincke rotation etc. [12–16]. In addition, some new mechanisms have been reported, which are known as liquid crystal enabled electroosmosis (LCEEO) and liquid crystal enabled electrophoresis (LCEEP). In the case of LCEEO, the asymmetric ion flow leads to the pumping of liquid crystal around static particles, whereas in LCEEP the particles are free to be transported [17–23]. In all these effects the anisotropic physical properties of the medium, the director orientation as well as the induced defects play a crucial role. It has been shown that no electrophoretic mobility is observed for spherical microparticles with quadrupolar director configuration such as Saturn ring and Boojum defects due to the symmetric ion flow [17]. However, the ion flow becomes asymmetric for spherical microparticles with dipolar configuration. Although there are a few studies reported on the orientation, interaction, and induced defects by nonspherical particles, the electrokinetic studies of anisotropic microparticles in the nematic liquid crystals are rare [23]. In this paper, we report the electrokinetics of birefringent microsheets in nematic liquid crystals. We show that the microsheets propel along the director and spin around its long axis under ac electric fields. The velocity of propelling and the angular frequency of spinning is controlled by the amplitude and frequency of the applied electric field.

II. EXPERIMENT

The organic microsheets were prepared as per the reported procedure [24]. It grows either in rectangular or hexagonal shape. We have used 5,10,15,20-tetra(p-tolyl) porphyrin as a building block to prepare nearly monodispersed microsheets. Figure 1 shows the optical microscopy image of a few number of microsheets on the glass slide. The microsheets are crystallized in tetrahydrofuran (THF) or THF/H_2O solvents. The microsheets lengths and widths are in the range of 9 to 10 μm and 4 to 5 μm, respectively. The average thickness of the microsheet is about 500 nm. The microsheets have a monoclinic crystal structure [24] and are optically birefringent [25]. They are emitting fluorescence light at wavelengths 719 and 653 nm upon excitation at 488 nm.

The microsheets are dispersed in liquid crystal by physical mixing. In the present study we used 5CB liquid crystal having positive dielectric anisotropy ($\Delta\epsilon = 9.6$) [26] and MLC-6608 exhibiting negative dielectric anisotropy ($\Delta\epsilon = -4.2$). The experimental cells with required spacing were fabricated by using indium-tin-oxide (ITO)-coated glass plates that are spin coated with polyimide AL-1254 and cured at 180°C for 1 h. They were rubbed antiparallel way for homogeneous alignment of the nematic director. For homeotropic alignment, we used JALS-204 and cured at 200°C for 1 h. Sinusoidal voltage was applied across the ITO electrodes of the cell using a function generator (Tektronix-AFG 3102) and a voltage amplifier (TEGAM-2350). The direction of the applied field was perpendicular to the cell substrates. All the experiments are done using ac electric field. The sample was observed using an inverted microscope (Nikon eclipse Ti-U). The trajectories of the particles were video recorded using a CCD camera (Pixelink PLB 741F) and an appropriate computer

*sdsp@uohyd.ernet.in

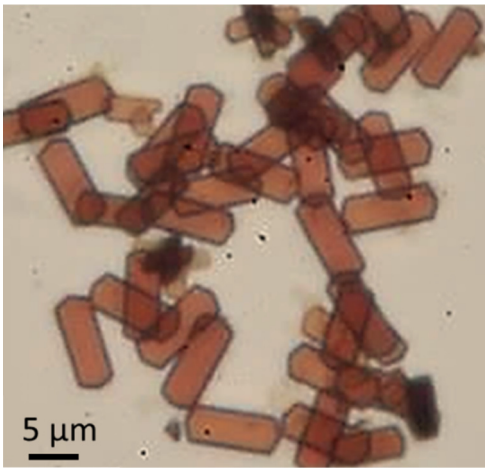

FIG. 1. Optical microscopy image of hexagonal single crystal microsheets.

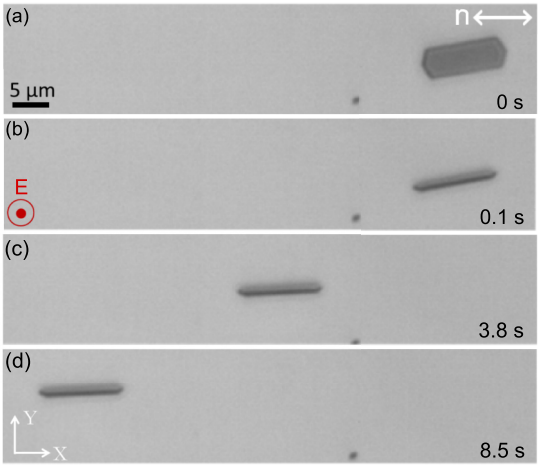

FIG. 2. (Top view) Electric-field-driven propelling of a microsheet in a planar nematic cell with negative dielectric anisotropy liquid crystal (MLC 6608) (see Supplemental Material S1: video 1 [29]). (a–d) Sequence of CCD images of the microsheet taken at different times and at applied field, $E = 2.8\ \mathrm{V}/\mu\mathrm{m}$ and frequency, $f = 1$ kHz. Cell thickness $d = 15\ \mu$m. Double-headed arrow at the right corner indicates the director and the electric field direction is out of plane.

program was used to track the trajectories of the microsheets. The orientation, interaction, and laser-assisted self-assembly of the microsheets in nematic liquid crystal is reported in our previous studies [25]. The microsheets induce tangential anchoring (without any coating) of liquid crystal molecules on the surface. Experimentally, it is difficult to identify the effective shape of the defects such as being points or loops around the microsheets. Dontabaktuni *et al.* have shown by Landau de Gennes Q-tensor modeling that in the case of platelet-shaped particles, for strong anchoring, the defect cores are at the edges of the platelets and for weak anchoring the defects virtually sink inside the platelets [27]. In fact, they showed that for the weak anchoring the defect are spread as quasidefect line along the edges. In the present case the anchoring is weak and similar defect structure is consistent with the experimental observation. We also studied the multiaxis rotations of the microsheets in both the isotropic and nematic phase of liquid crystals recently [28].

III. RESULT AND DISCUSSION

A. Electric-field-driven propelling

First, we discuss the electric-field-driven propelling of the microsheets in a negative dielectric anisotropy nematic liquid crystal (MLC-6608). In this case a planar cell was chosen and the direction of the applied field is perpendicular to the substrates. At zero field the plane of the microsheet is parallel to the cell substrates [Fig. 2(a)]. The long axes of the microsheets makes about 30° angle with respect to the rubbing direction. This was supported by Landau de Gennes Q-tensor modeling and reported in our previous studies [25]. When the electric field strength is increased the microsheet first rotates about the long body axis beyond a field amplitude of $0.2\ \mathrm{V}/\mu\mathrm{m}$ [Fig. 2(b)]. The short axis of the microsheet is now along the field direction. This rotation is due to the electric-field-induced torque [28]. When the field is increased beyond $1\ \mathrm{V}/\mu\mathrm{m}$, it starts to move along the x axis [Figs. 2(c) and 2(d)]. The long axis of the moving microsheet is tilted with respect to the substrates. A video clip of the particle transport is provided in the Supplemental Material (S1: video 1) [29].

The transport properties of the microsheet is characterized by measuring the linear velocity as a function of applied electric field and the driving frequency. Figure 3(a) shows the time-dependent position. The linear variation suggests that it moves with a uniform velocity. We measured the velocity (v) at various applied electric fields. Figure 3(b) shows that beyond a threshold field ($1\ \mathrm{V}/\mu\mathrm{m}$), v varies quadratically with the applied field. It may be mentioned that no transport is observed in the isotropic phase. Similar behavior was observed in the case of spherical water microdroplets with a point defect (dipolar configuration) in a negative dielectric anisotropy nematic liquid crystal [22,23]. It has been shown that the anisotropic character of the liquid crystal and the spatially varying director distortion around the spherical microparticle with hyperbolic hedgehog leads to liquid crystal enabled electrophoresis (LCEEP) [13,17,18,21]. In that case the mobile ions of liquid crystal move in opposite directions due to the Coulomb force and the ionic mobility parallel to the local director is different from that of the perpendicular direction. The associated electro-osmotic flows are different in the two opposite sides of the particle and the mirror symmetry of electro-osmotic flow is broken. Therefore, the flow is stronger on one side of the microsphere and consequently it moves toward the opposite side with a velocity given by: $|v| = \frac{\alpha\epsilon_o\bar{\epsilon}R}{\eta}[|\frac{\Delta\sigma}{\bar{\sigma}} - \frac{\Delta\epsilon}{\bar{\epsilon}}|]E^2$, where α is a constant and depends on the director configuration, R is the size of the particle, η is the average viscosity, $\bar{\sigma}$ is the average conductivity, and $\bar{\epsilon}$ the average dielectric constant [17,20,21]. It should be noted that for microparticles with Saturn ring and Boojum defects, the director configuration is quadrupolar, which preserves the fore-aft symmetry of the ion flow and results in zero electrophoretic mobility.

We further studied the frequency dependence of the liquid crystal enabled electrophoretic velocity of the microsheets.

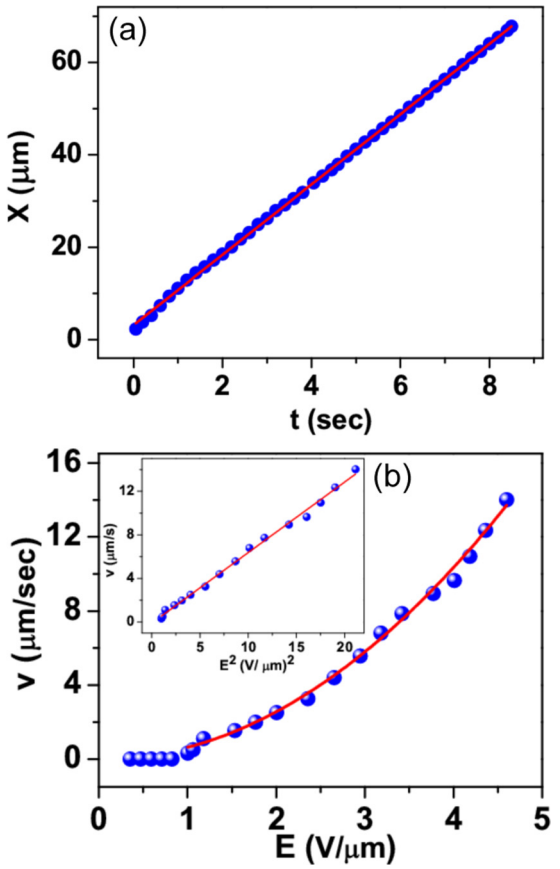

FIG. 3. (a) The time-dependent position of a microsheet at a fixed field strength $E = 3.4\,\mathrm{V}/\mu\mathrm{m}$. (b) Electrophoretic velocity v as a function of the applied electric field at a fixed frequency $f = 1\,\mathrm{kHz}$. Cell thickness $d = 15\,\mu\mathrm{m}$. The red line is the best fit to $v \propto E^2$. (Inset) The linear variation of v with E^2.

Figure 4 shows the frequency dependence of transport velocities for two different field amplitudes namely, $E = 3.2\,\mathrm{V}/\mu\mathrm{m}$ and $4\,\mathrm{V}/\mu\mathrm{m}$. They exhibit broad maxima and the propulsion

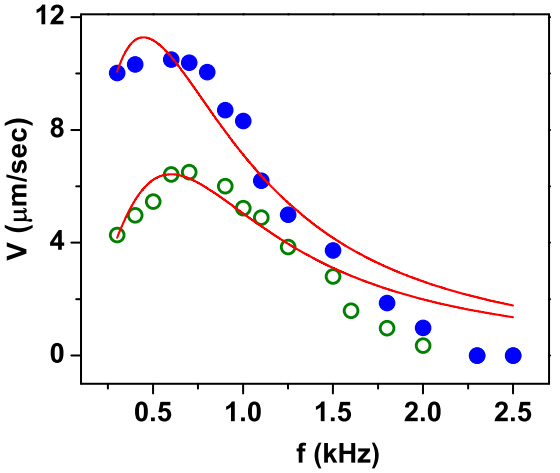

FIG. 4. Variation of velocity as a function of applied frequency at two different fixed field strengths, $E = 3.2\,\mathrm{V}/\mu\mathrm{m}$ (green open circles) and $E = 4\,\mathrm{V}/\mu\mathrm{m}$ (filled blue circles), respectively. Cell thickness $d = 15\,\mu m$. The continuous red lines are the best fits to Eq. (1).

ceases to exist at both higher and lower frequencies. In particular, the velocity is zero below 450 Hz and above 2.5 kHz. The frequency dependence of the induced charge electrophoretic flow has been studied for spherical microdroplets and microparticles [21,22]. The flow is described by

$$v(\omega) = v_o \frac{\omega^2 \tau_e^2}{(1+\omega^2\tau_p^2)(1+\omega^2\tau_e^2)}, \tag{1}$$

where $\omega = 2\pi f$, $\tau_p = \lambda_D L/2D$ is the particle charging time and $\tau_e = \lambda_D d/2D$ is the electrode charging time. λ_D is the Debye screening length, D is the diffusion coefficient of the ions, and L is the particle size. The frequency dependence of the microsheets shows a generic behavior, i.e., similar to that of spherical particles [22]. Therefore, it may be legitimate to use the same model for analysis. The experimental data is fitted with Eq. (1), and the continuous red lines in Fig. 4 show the best fits to the data. At higher frequency a small discrepancy in the fitting may be partially due to the change in values of $\Delta\epsilon$ and $\Delta\sigma$ of the liquid crystal with frequency. The fit parameters are $\tau_p = 5 \times 10^{-4}$ s and $\tau_e = 2 \times 10^{-3}$ s. The corresponding lower and upper cutoff frequencies are given by $f_l = \tau_e^{-1} \approx 450$ Hz and $f_u = \tau_p^{-1} \approx 2$ kHz. These cutoff frequencies are very close to the experimental values despite the very different shape of the particle. One quantitative difference with the previous studies on spherical microparticles is that here the frequency range is much larger.

The quadratic variation of velocity with the electric field and their frequency dependence clearly suggests that the microsheets propel due to symmetry breaking ion flow. We propose a possible mechanism by which the symmetric ion flow around the microsheets can be broken. From our previous studies we know that the director distribution has an asymmetry along the y axis (perpendicular to the rubbing direction) as shown in Fig. 5(a) [25]. In particular, the distortion is stronger on the right side of the microsheet than the left side. Figure 5(b) shows the schematic side view (after the rotation) of the microsheet when the electric field is applied ($>1\,\mathrm{V}/\mu\mathrm{m}$). In this case the microsheet is tilted with respect to the substrate and one corner is closer to the bottom substrate than the other. The strongest distortions of director are at the corners and

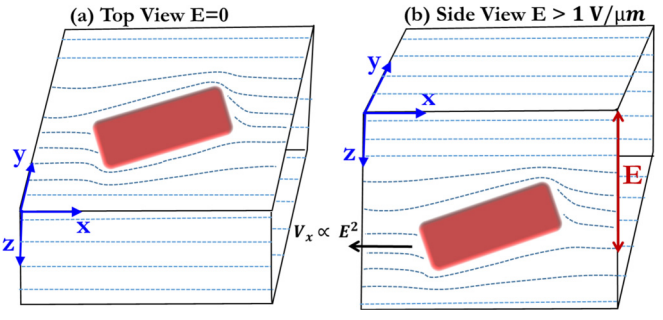

FIG. 5. (a) Schematic top view of a microsheet in a planar aligned nematic at $E = 0$. Here the plane of the microsheet is parallel to x-y plane. The director field surrounding the microsheet is shown with dotted lines. (b) Schematic side view when the field is applied along the z axis and $E > 1\,\mathrm{V}/\mu\mathrm{m}$, the microsheet rotates along the x axis and its plane becomes parallel to x-z. The black arrow indicates the transport direction of the microsheet.

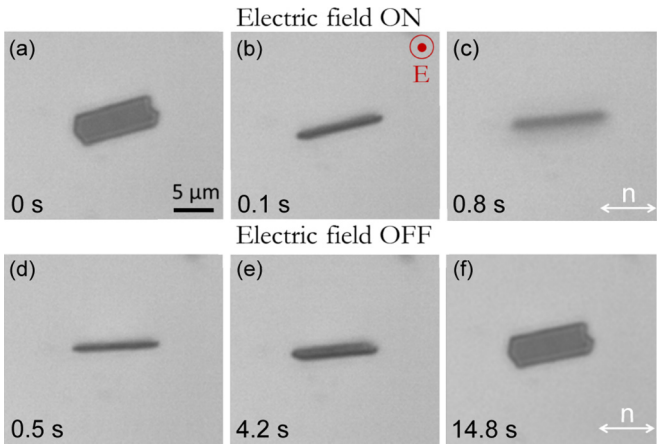

FIG. 6. Electric field response of microsheet at higher frequency ($f = 100$ kHz). Applied field amplitude $E = 3.5\,\mathrm{V}/\mu\mathrm{m}$. (b) The microsheet first rotates and the short axis of the sheet is now along the field direction. (c) The microsheet moves toward the bottom substrate and goes out of focus (see Supplemental Material S2: video 2). (d–f) Returning back to the previous position after switching off the field.

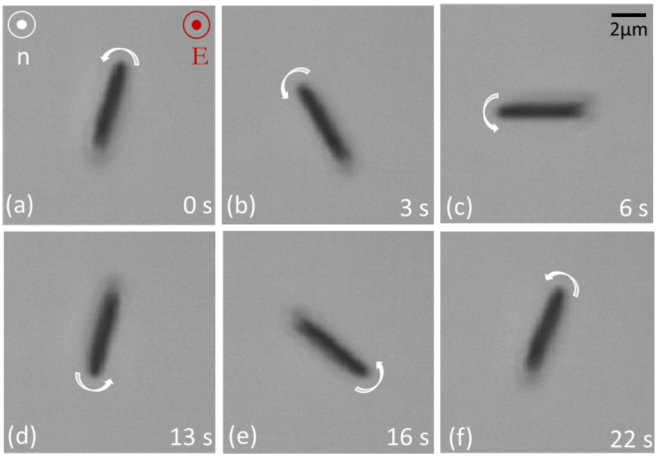

FIG. 7. Electric-field-driven spinning of a microsheet in a homeotropic cell with 5CB nematic liquid crystal (see Supplemental Material S3: video 3). (a–f) Sequence of CCD images of the microsheet taken at different times at field amplitude $E = 0.85\,\mathrm{V}/\mu\mathrm{m}$ and frequency, $f = 1$ kHz. $\hat{n}$ is the director and the field direction is out of the plane. White arrows indicate the direction of rotation. Cell thickness $d = 20\,\mu$m.

these regions are enriched with positive and negative ions. The applied electric field exerts a bulk force on the charge cloud, which leads to the flow of ions in the opposite directions and the flow pattern follows the director structure. The flow of ions is stronger at the right side of the microsheet, which pushes the particle in the left side [black arrow in Fig. 5(b)]. The microsheet is propelled along the negative direction of the x axis when it is tilted counterclockwise with respect to the director. Similarly, it moves along the positive x direction when tilted in the clockwise direction. Thus, tilting of the microsheet and the asymmetric director orientation can break the symmetry of the ion flow.

At much higher frequencies of the electric field [larger than the upper cutoff frequency, $f_u \simeq 2.5$ kHz (see Fig. 4)], we observed a change in the vertical position of the microsheet with respect to the bottom substrate. In this case we applied an electric field of amplitude 3.5 V/μm and frequency 100 kHz and observed the response of a microsheet with time after switching on and switching off the field. Figure 6 shows that when the field is switched on the microsheet first rotates and tend to align the short axis along the field direction [Fig. 6(b)] and then goes down toward the bottom substrate with increasing time [Fig. 6(c)]. A video clip of the particles movement showing that it goes out of focus toward the bottom surface is provided in the Supplemental Material (S2: video 2) [29]. Once the field is switched off, the microsheet comes back to its original position due to the liquid-crystal-enabled levitation [Figs. 6(d)–6(f)] [13]. A similar kind of net displacement was observed for colloidal fullerenes in a nematic liquid crystal [3]. It is suggested that if the frequency of the electric field is greater than the frequency corresponding to the particle charging time, a net dipole moment is induced and the particles can get attracted toward the electrodes. In the present experiment it always move toward the bottom substrate and this is probably due to the fact that the microsheets are closer to the bottom substrate.

B. Electric-field-driven spinning

Further, we studied the electric-field response of the microsheets in homeotropic cells with positive dielectric anisotropy nematic liquid crystal (5CB). The microsheet is standing with respect to the substrate surface. From the computer simulation in our previous studies we found that the long axis of the microsheet is tilted with respect to the vertical direction by an angle of 22° [25]. When the ac electric field is applied we observed that the microsheet becomes vertical and continuously spins about the field direction. The spinning direction could be either clockwise or counterclockwise. Some sequence of images at different times of a microsheet is shown in Fig. 7. A video clip showing the spinning of three microsheets in both clockwise and counterclockwise directions is provided in the Supplemental Material (S3: video 3) [29]. We measured the angular frequency of spinning at various fields at a fixed frequency of the electric field. Figure 8(a) shows that the angular frequency varies quadratically with the electric field beyond a threshold field (0.2 V/μm). We also measured the dependence of the spinning frequency on the driving frequency of the electric field at a fixed value ($E = 1.5\,\mathrm{V}/\mu\mathrm{m}$). Figure 8(b) shows that the spinning frequency decreases rapidly with increasing the driving (field) frequency and finally becomes zero. It varies almost inversely with the driving frequency (i.e., $\omega \propto 1/f$) up to 2 kHz and then changes slope at 2.5 kHz and finally goes to zero at 3 kHz. Here the upper cutoff frequency (3 kHz) is connected to the particle charging time and this is almost comparable to the upper cutoff frequency for the linear transport. When the field is switched on in the isotropic phase, no sustained spinning was observed, although it shows a tendency to spin but stops immediately (see Supplemental Material, S4: video 4 [29]). This could be due to the sedimentation of the microsheets. In the nematic phase the rotation is sustained because the microsheets are pushed away from both the plates due to the antagonistic director alignment

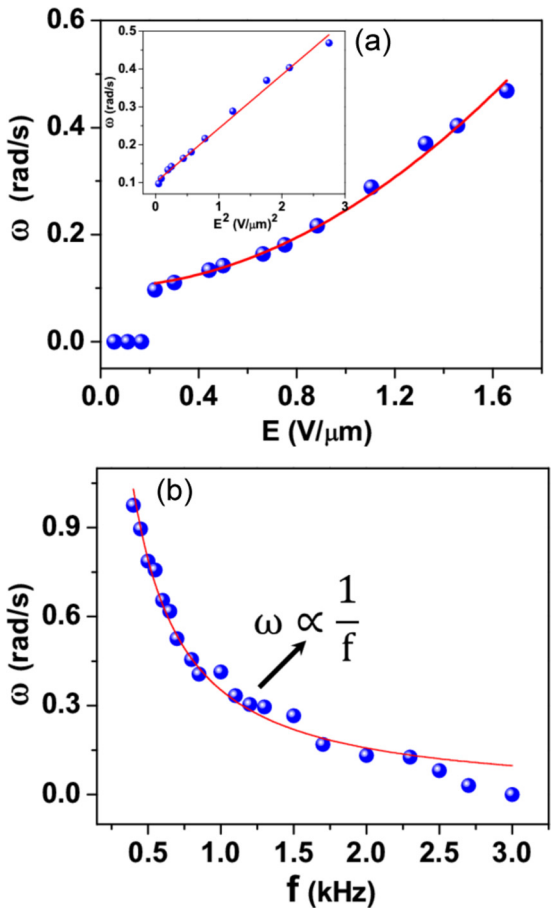

FIG. 8. (a) Variation of angular frequency of spinning of a microsheet as a function of the applied electric field. The driving frequency is $f = 1$ kHz. The solid red line is the best fit to $\omega \propto E^2$. (Inset) Linear variation of ω with E^2. (b) Variation of angular frequency of spinning as a function of driving frequency of the field ($E = 1.5$ V/μm). Red line shows the best fit to $\omega \propto 1/f$.

at the top and bottom sides of the microsheet with respect to the plates [13]. It may be mentioned that this rotation is very different than the Quincke rotation, which is observed under dc field, where the axis of rotation is perpendicular to the field direction [14].

Under normal condition a uniform ac electric field cannot generate continuous rotation because sustained rotation requires a rotating external field. However, there are some theoretical and experimental studies reported on the electrokinetics of microparticles under ac field in isotropic fluids [6,8–10,30]. Bazant and coworkers have shown theoretically that breaking spatial symmetry generically leads to an ICEO pumping flow that can give rise to either directional motion or steady rotation of free particles in isotropic fluids [4,5,11]. They have studied in great details on objects with various shapes and surface properties, and the angular frequency of colloidal rotation shows quadratic field dependence [6,30]. Subsequently, there have been some experimental studies showing the rotation of Janus doublets, microvalves, microrod, etc., under ac electric field [6,8,31]. From the field and frequency dependence of spinning the microsheets it is clear that the spinning is due to the ICEO as described by Bazant and coworkers. Although the shape of our particle is very different than those used in previous theoretical and experimental studies the basic mechanism (ICEO) appears to be the same. Further studies are needed to understand the system quantitatively.

IV. CONCLUSION

In conclusion, we have studied the electric-field-induced propelling and spinning of microsheets in nematic liquid crystals. These microsheets are optically anisotropic. In planar-aligned liquid crystals with negative dielectric anisotropy, the electric field does not reorient the director but the microsheet propels parallel to the director. The propelling velocity varies quadratically with the electric field. The frequency dependence of the microsheet's velocity exhibits a maximum and the propulsion ceases above a particular frequency. We proposed a mechanism of asymmetric ion flow around the microsheets that accounts for the observed propulsion. We observed sustained spinning of microsheets driven by ac electric field in homeotropic cells with positive dielectric anisotropy liquid crystals. The angular frequency of spinning is proportional to the square of the applied field and decreases rapidly with increasing frequency of the electric field and finally ceases beyond a particular frequency. The diversity and complexity of electrokinetics of colloids are interesting and promising and we hope this study will invoke more studies on highly shape anisotropic microparticles.

ACKNOWLEDGMENTS

We gratefully acknowledge the support from the Department of Science and Technology (Grant No. DST/SJF/PSA-02/2014-2015), and DST-PURSE. M.V.R. acknowledges UGC-BSR for support through a fellowship grant.

[1] A. Ramos, *Electrokinetics and Electrohydrodynamics in Microsystems* (Springer, Vienna, 2011).
[2] H. Morgan and N. G. Green, *AC Electrokinetics: Colloids and Nanoparticles* (Research Studies Press, Philadelphia, PA, 2003).
[3] A. K. Srivastava, M. Kim, S. M. Kim, M. K. Kim, K. Lee, Y. H. Lee, M. H. Lee, and S. H. Lee, Phys. Rev. E **80**, 051702 (2009).
[4] T. M. Squires and M. Z. Bazant, J. Fluid Mech. **509**, 217 (2004).
[5] T. M. Squires and M. Z. Bazant, J. Fluid Mech. **560**, 65 (2006).
[6] A. Boymelgreen, G. Yossifon, S. Park, and T. Miloh, Phys. Rev. E **89**, 011003(R) (2014).
[7] S. Gangwal, O. J. Cayre, M. Z. Bazant, and O. D. Velev, Phys. Rev. Lett. **100**, 058302 (2008).
[8] H. Sugioka, Phys. Rev. E **81**, 036301 (2010).
[9] K. A. Rose, J. A. Meier, G. M. Dougherty, and J. G. Santiago, Phys. Rev. E **75**, 011503 (2007).
[10] E. Yariv, Phys. Fluids **17**, 051702 (2005).

[11] M. Z. Bazant and T. M. Squires, Phys. Rev. Lett. **92**, 066101 (2004).
[12] Y. Sasaki, Y. Takikawa, V. S. R. Jampani, H. Hoshikawa, T. Seto, C. Bahr, S. Herminghaus, Y. Hidakac, and H. Orihara, Soft Matter **10**, 8813 (2014).
[13] O. D. Lavrentovich, Soft Matter **10**, 1264 (2014).
[14] G. Liao, I. I. Smalyukh, J. R. Kelly, O. D. Lavrentovich, and A. Jakli, Phys. Rev. E **72**, 031704 (2005).
[15] I. Dierking, G. Biddulph, and K. Matthews, Phys. Rev. E **73**, 011702 (2006).
[16] A. Jakli, B. Senyuk, G. Liao, and O. D. Lavrentovich, Soft Matter **4**, 2471 (2008).
[17] O. D. Lavrentovich, Curr. Opin. Colloid Interface Sci. **21**, 97 (2016).
[18] O. D. Lavrentovich, I. Lazo, and O. P. Pishnyak, Nature **467**, 947 (2010).
[19] I. Lazo, C. H. peng, J. Xiang, S. V. Shiyanovskii, and O. D. Lavrentovich, Nat. Commun. **5**, 5033 (2014).
[20] C. Peng, Y. Guo, C. Conklin, J. Vinals, S. V. Shiyanovskii, Q. H. Wei, and O. D. Lavrentovich, Phys. Rev. E **92**, 052502 (2015).
[21] I. Lazo and O. D. Lavrentovich, Philos. Trans. R. Soc. A **371**, 20120255 (2013).
[22] S. H. Navarro, P. Tierno, J. I. Mullol, and F. Sagues, Soft Matter **9**, 7999 (2013).
[23] S. Hernàndez-Navarro, P. Tierno, J. Ignés-Mullol, and F. Sagués, Eur. Phys. J. Spec. Top. **224**, 1263 (2015).
[24] N. Chandrasekhar, S. Basak, M. A. Mohiddon, and R. Chandrasekhar, ACS Appl. Mater. Interfaces **6**, 1488 (2014).
[25] M. V. Rasna, K. P. Zuhail, U. V. Ramudu, R. Chandrasekar, J. Dontabhaktunic, and Surajit Dhara, Soft Matter **11**, 7674 (2015).
[26] R. Manda, V. Dasari, P. Sathyanarayana, M. V. Rasna, P. Paik, and S. Dhara, Appl. Phys. Lett. **103**, 141910 (2013).
[27] J. Dontabhaktuni, M. Ravnik, and S. Zumer, Soft Matter **8**, 1657 (2012).
[28] M. V. Rasna, K. P. Zuhail, U. V. Ramudu, R. Chandrasekar, and Surajit Dhara, Phys. Rev. E **94**, 032701 (2016).
[29] See Supplemental Material at http://link.aps.org/supplemental/10.1103/PhysRevE.95.012710 for multimedia videos and video descriptions.
[30] J. S. Solano, D. T. Wu, and D. W. M. Marr, Langmuir **22**, 5932 (2006).
[31] G. Yossifon, I. Frankel, and T. Miloh, Phys. Fluids **19**, 068105 (2007).